35th Annual International Conference of the IEEE EMBS
Osaka, Japan, 3 - 7 July, 2013

Quantitative Elastography and its Application to Blood Pressure Estimation: Theoretical and Experimental Results

Aaron M. Zakrzewski and Brian W. Anthony

Abstract— **Elastography is a method that can be used to measure the elasticity of soft biological tissue and, ultimately, to detect cancerous tumors. In this paper, quantitative elastography is developed using a fast multi-scale approach. Results are presented in simulation and preliminary results are presented in experiment. The optimization methods of elastography are applied to measure noninvasively the arterial wall stiffness of a vessel as well as blood pressure. Simulation results are presented that confirm the accuracy of methods, and preliminary experimental results are presented that measure pressure within a cylindrical cavity in a phantom. Using ultrasound, these methods could provide noninvasive continuous measurement of blood pressure in major arteries and could give doctors another method with which to gather information about a patient's cardiovascular health.**

I. Introduction

It is well known that cancerous tumors have a higher elastic modulus than the surrounding healthy tissue. First described in 1991 by Ophir, elastography is a computational method that measures the elasticity of soft biological tissue and thus can detect cancerous breast tumors [1]. Quantitative elastography is performed by first measuring the displacement between an uncompressed and a compressed ultrasound B-Mode image. The known displacement distribution and the measured applied force are inputs to a fast multi scale nonlinear optimization algorithm that solves the associated inverse problem and calculates the tissue elasticity distribution.

This procedure is used as a basis to measure noninvasively blood pressure in major arteries. Current noninvasive blood pressure estimation occurs through tonometry, pulse wave velocity, blood pressure cuffs, and finger cuffs, among other methods. Pulse wave velocity requires two points of measurement and does not give results for patients with artificial hearts because artificial hearts often do not have dynamic pressure pulses [2]. Appalation tonometry is able to give accurate estimates of central blood pressure, but also requires two simultaneous measurements to be made [3]. Blood pressure cuffs cut off blood flow to a limb and thus are not suitable for continuous estimation of blood pressure. Finger cuffs are known to be inaccurate and can only provide estimates of blood pressure at the periphery, which varies greatly from the central blood pressure [3]. The method described in this paper will be able to give accurate and continuous results for both artificial hearts and normal dynamic blood flow, while using only one measurement site, such as at the carotid artery.

The algorithm also obtains a quantitative measurement of arterial wall stiffness. Augmentation index is a well-developed method that gives a qualitative noninvasive estimation of artery stiffness, while pulse wave velocity can calculate a quantitative estimation of arterial wall stiffness [4]. However, pulse wave velocity suffers from the disadvantages stated above. The novel method presented in this paper will give quantitative values using known information directly available with an ultrasound probe.

To the authors' knowledge, the only application of elastography methods to blood pressure and arterial wall stiffness estimation is that by Zakrzewski *et al.* [5]. The current paper uses a similar theory and further develops and verifies the methods.

II. Theory

A. Elasticity Reconstruction

In simulation, uncompressed and compressed ultrasound B-Mode images are obtained using a Matlab program named Field II in conjunction with the commercially available finite element program Abaqus to model the physics of the tissue compression [6] [7]. The tissue is compressed by approximately 5 percent of the axial length of the tissue and a multi-scale block-matching method, as described by Sun *et al.*, estimates the displacement between each pair of ultrasound B-Mode images [8]. The gradient of the displacement distribution forms the strain image, which indicates an approximate qualitative elasticity map.

From the displacement image and the known applied force, the inverse problem can be solved in Matlab for the tissue elasticity as a function of location within the tissue. See Figure 1 for a flow chart of the inverse problem solution. The Levenberg-Marquardt method is used for the nonlinear optimization with objective function

$$F(x) = (x-x_0)^T(x-x_0) \quad (1)$$

where x is a vector containing the axial displacement at each node of the finite element mesh in the problem and x_0 is the known axial displacements obtained from the block-matching method described above. To solve the inverse problem, the optimization step is defined by

The authors are with the Laboratory of Manufacturing and Productivity, Mechanical Engineering Department, Massachusetts Institute of Technology, Cambridge, MA 02139 USA (e-mail: azakrzew@mit.edu).

978-1-4577-0216-7/13/$26.00 ©2013 IEEE

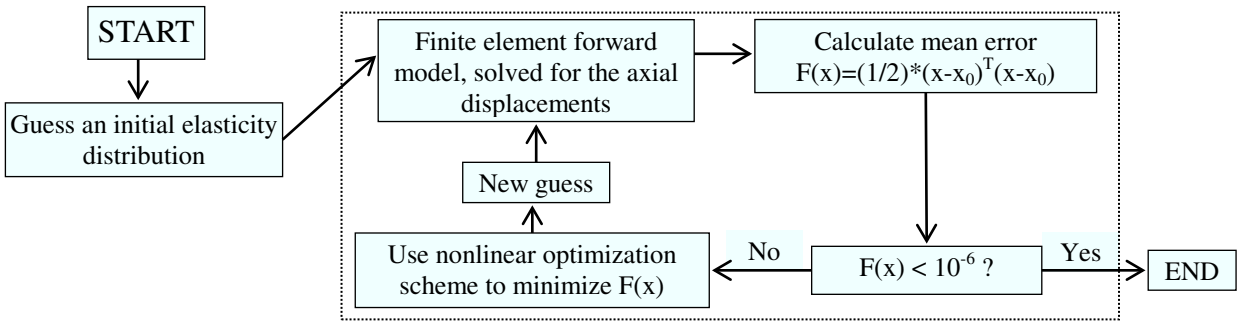

Figure 1. Flow chart showing the solution approach to the inverse problem.

$$\Delta x = (J^T J+\lambda I)^{-1}(J^T(x-x_0)) \quad (2)$$

where J is the n x m Jacobian matrix, m is the number of elements in the mesh, n is the number of nodes, λ is the Marquardt parameter, and I is the identity matrix.

In order to compute the Jacobian matrix, finite element analysis is used and a backward difference method is used to calculate the derivative. Linear quadrilateral mesh generation occurs in Matlab, with mesh smoothing algorithms implemented as described by Blacker *et al.* [9]. A linear, isotropic material under plane strain conditions is assumed for this study with a Poisson ratio of 0.495.

A multi-scale optimization approach, as demonstrated in Figure 2, is used such that the problem is initially solved on a coarse mesh. If the error in the objective function changes by less than 1 % between iterations, the mesh automatically refines and the problem continues on the new mesh. The algorithm stops when the error is less than $1x10^{-6}$ or when the elasticity map does not change after many successive mesh refinements. This multi-scale approach is advantageous because it serves to reduce the number of Jacobian calculations, which is the most computationally expensive portion of the algorithm. Where applicable, by-hand segmentation is used to identify the inclusions in the phantom materials.

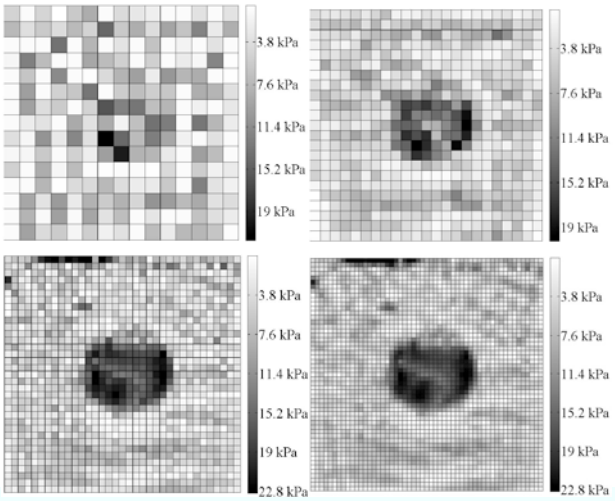

Figure 2. Demonstration of the multi-scale approach used. The mesh refines automatically from coarse to fine throughout the optimization process.

B. *Blood Pressure Estimation*

With the current methods, arterial wall stiffness, blood pressure, and bulk tissue stiffness are simultaneously measured. The artery is modeled in finite elements using truss elements and the blood is modeled using a pressure boundary condition on the vessel wall. The truss elements increase the speed of the solution because they do not require costly mesh transitions between the artery and the bulk material. The displacement results of the truss element agree closely with a finely meshed artery of plane strain elements. The vessel is prescribed to have the same displacements as the immediately surrounding bulk tissue, and blood pressure is assumed constant in the vessel. Realistic values for arterial wall stiffness and blood pressure are used, 400 kPa and 80 mmhg, respectively.

The displacement tracking techniques, described in the previous section, measure tissue displacement in this case. To account for pressure and arterial wall stiffness in the inverse problem, the vector of optimization variables extends to include these two additional variables. Reasonable limits are placed on the variables to ensure a viable solution and smoothing is used after each iteration in order to get realistic results. Due to the highly coupled nature of blood pressure and arterial wall stiffness with respect to tissue displacement, a good quality mesh around the vessel is important in order to get accurate results for both the blood pressure and arterial wall.

III. EXPERIMENT

A. *Elasticity Reconstruction*

For the elasticity reconstructions, gelatin phantoms are

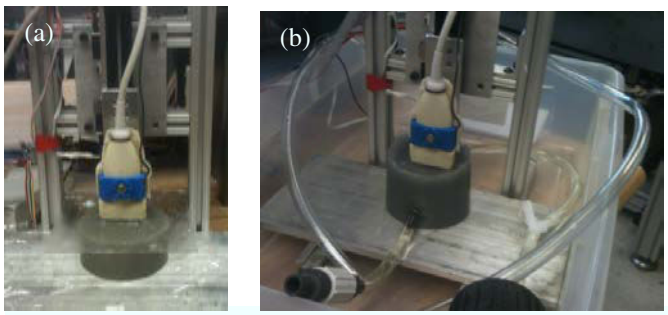

Figure 3. Experimental set-up for (a) the elasticity reconstruction and (b) water pressure estimation.

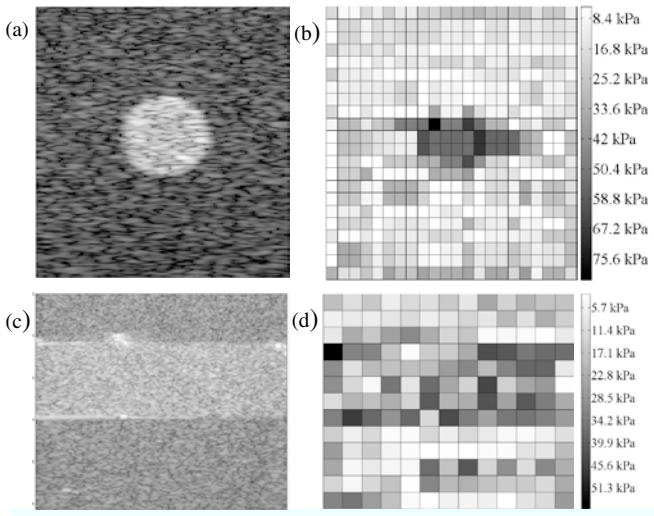

Figure 4. Results of the elasticity reconstruction. (a)-(b) show the simulation results while (c)-(d) show the experimental results. B-Mode images and elasticity reconstructions are shown.

constructed according to the methods presented by Hall *et al.* [10]. For each experimental test, a compression-test phantom and an elastography phantom are made. In the experiments shown, the inclusion contains 5 percent graphite powder scatterers while bulk material contains 1 percent graphite powder scatterers. For the inclusion phantoms, a negative mold creates a hole in the material such that the bulk material congeals first and the inclusion then is poured into the mold. Phantoms have a diameter of 60 mm and a height of 60 mm, and inclusions have a diameter of 9.525 mm.

A 7L3V Terason ultrasound probe with 128 elements is used, with the associated software development kit (SDK), to gather the relevant radio frequency (RF) data. A force measurement probe attachment, as described by Gilbertson *et al*, is used in order to gather the information necessary to solve the inverse problem and an actuator is used to measure accurately the probe displacement during the experiments [11]. This attachment conforms to the contours of the ultrasound probe and is appropriate for clinical use. An acrylic compression plate with a tightly fitting hole for the ultrasound probe ensures that the force is applied over the entire top surface of the phantom. Figure 3a shows the experimental set-up.

B. Blood Pressure Estimation

As in the previous section, the experiment requires two cylindrical phantoms – one compression-test phantom, and one phantom containing a vessel with a diameter of 9.525 mm. For these experimental tests, copolymer-in-mineral-oil cylindrical phantoms are made according to the methods presented by Oudry *et al.* [12]. Water takes the place of blood and, in these preliminary results, the arterial wall is neglected in order to prove the ability of the algorithm to estimate pressure. The experiment considers the static case and the height of a water column measures the pressure within the vessel. The results are relevant in the non-static case because B-Mode images will be automatically recorded at the maximum lumen diameter (systole) and the minimum lumen diameter (diastole). The setup is shown in Figure 3b.

IV. Results

A. Elasticity Reconstruction

Elastography with a stiff inclusion was performed in simulation and on experimental phantoms. Relevant B-Mode images and elasticity images are shown in Figure 4, where (a)-(b) represent theory and (c)-(d) represent experimental results. In the experimental data, the cylindrical inclusion, as shown, is imaged along the axis of the cylinder. Theoretically, the elasticity of the bulk tissue is measured to 1.9 percent error and the elasticity of the inclusion is measured to 7.2 percent error. Experimentally, the bulk tissue is measured to 1.9 percent error and the inclusion to 1.7 percent error. The signal to noise ratio (SNR) is defined as

$$\mathrm{SNR} = s/\sigma \tag{3}$$

where s is the mean elasticity of the region of interest and σ is the standard deviation. In the simulated data, the SNR is measured as 1.6 for the bulk material and 1.7 for the inclusion. The SNR for the experiments is 2.3 for the inclusion and 1.5 for the bulk tissue. The contrast ratio is defined as

$$\gamma = |\log(C_E)| - |\log(C_T)| \tag{4}$$

where C_E is the elasticity contrast obtained from elastography and C_T is the true elasticity contrast. The contrast ratio is measured to be -0.093 in simulation and -

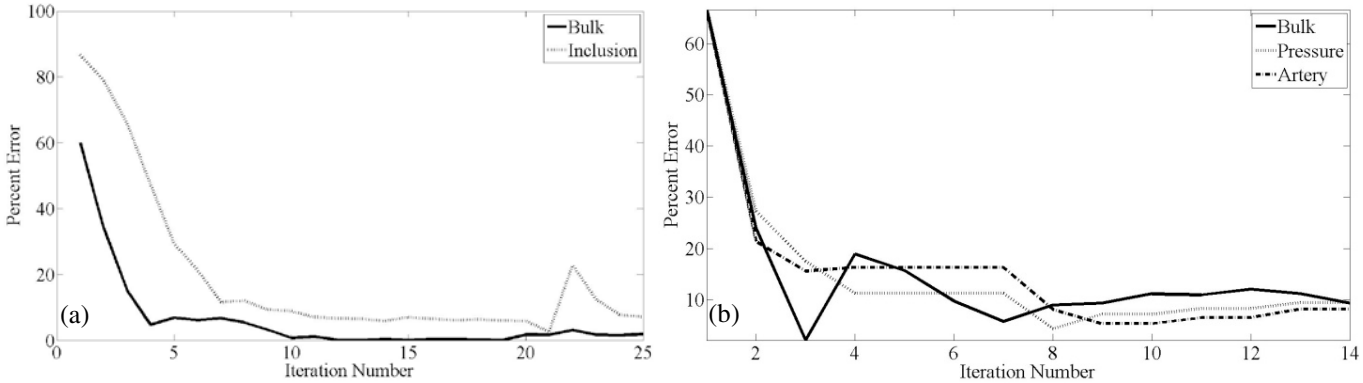

Figure 5. Convergence plots for the simulation results. (a) shows convergence of the elasticity reconstruction and (b) shows convergence of the water pressure reconstruction.

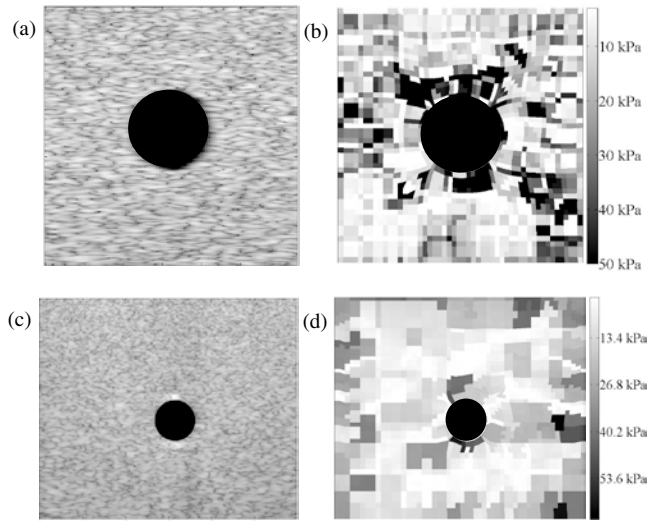

Figure 6. Results for blood pressure estimation. (a)-(b) show the simulation results, which include the arterial wall, while (c)-(d), show the experimental results, which neglect the arterial wall. B-Mode images and elasticity reconstructions are shown.

0.038 in experiment. In Figure 5a, the error of the reconstruction is plotted versus iteration number in simulation; overall, as the iteration number increases, the result converges. Note that upward spikes in the percent error are an artifact of the mutli-scale approach, which solves the problem on a completely new grid.

B. Blood Pressure Estimation

Blood pressure estimation was completed in theory with the arterial wall and in experiment without the arterial wall, as shown in Figure 6. The blood pressure, material elasticity, and arterial wall elasticity are measured in simulation to 9.4 percent, 9.2 percent, and 8.2 percent error, respectively, and the bulk elasticity is estimated with an SNR of 0.51. In order to obtain as accurate a result as possible, four image pairs were used in the optimization process. A convergence plot of the simulation is shown in Figure 5b, where it is clear that as the iteration number increases, the results converge. In experiment, the pressure is estimated to within 4.1 percent error and the elasticity is measured to 0.3 percent error. The SNR of the bulk tissue in experiment is 1.3.

The multi-scale approach is advantageous, especially during blood pressure estimation; with known elasticity of the material, blood pressure can be estimated in simulation within 15 seconds. The goal of this paper is to demonstrate the method and, therefore, the algorithms were not optimized for speed. With hardware and software optimization, this estimation should be able to be completed in real-time.

V. Conclusion

This work presented a novel method of blood pressure estimation that could lead to clinically relevant noninvasive, continuous blood pressure estimation. While the arterial wall was neglected, the arterial wall can be added in experiment using a very thin stiff material around the vessel wall and solving the inverse problem as in the simulations discussed. A future paper will apply these methods *in vivo*.

Acknowledgment

Kai Thomenius is gratefully acknowledged for his ideas for improving this work.

References

[1] J. Ophir, I. Cespedes, H. Ponnekanti, Y. Yazdi, and X. Li. "Elastography: a quantitative method for imaging the elasticity of biological tissues." *Ultrasonic Imaging*, vol. 13, pp. 111-134, 1991.

[2] K. Hirata, M. Kawakami, and M.F. O'Rourke. "Pulse wave analysis and pulse wave velocity: a review of blood pressure interpretation 100 years after Korotkov." *Circ J*, vol. 70, pp. 1231-1239, 2006.

[3] T.G. Pickering, J.E. Hall, L.J. Appel, B.E. Falkner, J. Graves, M.N. Hill, D.W. Jones, T. Kurtz, S.G. Sheps, and E.J. Roccella. "Recommendations of blood pressure measurement in humans and experimental animals. Part 1: blood pressure measurement in humans. A Statement for Professionals from the Subcommittee of Professional and Public Education of the American Heart Association Council on High Blood Pressure Research." *Circulation*, vol. 111, pp. 697-716, 2005.

[4] S. Laurent, J. Cockcroft, L. Van Bortel, P. Boutouyrie, C. Giannattasia, D. Hayoz, B. Pannier, C. Vlachopoulos, I. Wilkinson, and H. Struijker-Boudier. "Abridged version of the expert consensus document on arterial stiffness." *Artery Research*, vol. 1, no. 1, pp. 2-12, 2007.

[5] A.M. Zakrzewski, S.Y. Sun, M.W. Gilbertson, B. Vannah, L. Chai, J. Ramos, and B.W. Anthony. "Multi-scale compression-based quantitative elastography and its application to blood pressure estimation." in *International Tissue Elasticity Conference*, 2012.

[6] J.A. Jenson. "Field: a program for simulating ultrasound systems." in *10th Nordicbaltic Conference on Biomedical Imaging*, 1996, pp. 351-353.

[7] J.A. Jenson, and N.B. Svendsen. "Calculation of pressure fields from arbitrarily shaped, apodized, and excited ultrasound transducers." in *IEEE Transactions on Ultrasonics, Ferroelectrics, and Frequency Control*, 1992, pp. 262-267.

[8] S.Y. Sun, B.W. Anthony, and M.W. Gilbertson. "Trajectory-based deformation correction in ultrasound images." in *SPIE Medical Imaging: Ultrasonic Imaging, Tomography, and Therapy*, 2010.

[9] T.D. Blacker, and M.B. Stephenson. "Paving: A new approach to automated quadrilateral mesh generation." *International Journal for Numerical Methods in Engineering*, vol. 32, pp. 811-847, 1991.

[10] T.J. Hall, M. Bilgen, M.F. Insana, and T.A. Krouskop. "Phantom materials for elastography." in IEEE Transactions on Ultrasonics, Ferroelectrics, and Frequency Control, 1997, pp. 1355-1365.

[11] M.W. Gilbertson. "Handheld Force-Controlled Ultrasound." M.S. thesis, Massachusetts Institute of Technology, USA, 2010.

[12] J. Oudry, C. Bastard, V. Miette, R. Willinger, and L. Sandrin. "Copolymer in-oil phantom materials for elastography," *Ultrasound in Medicine and Biology*, vol. 35, no. 7, pp. 1185-1197, 2009.